Resistivity scaling in epitaxial $CuAl_2(001)$ layers

Minghua Zhang and Daniel Gall

***Abstract*—Epitaxial $CuAl_2(001)$ layers with thickness d = 10.2 - 141 nm are deposited by co-sputtering onto MgO(001) substrates at 300 °C and their resistivity ρ is measured *in situ* to quantify the $CuAl_2$ resistivity scaling. A combination of X-ray diffraction θ-2θ scans, ω rocking curves and φ-scans confirm the single crystal microstructure with a 45°-rotated epitaxy with $CuAl_2(001)$ || MgO(001) and $CuAl_2(100)$ || MgO(110). The measured ρ increases with decreasing d, which is well described by the Fuchs-Sondheimer model, yielding a room-temperature electron mean free path λ = 15.6 nm with a bulk resistivity ρ_o = 7.7 μΩ cm. The latter value is 18% above the previously reported ρ_o, which is attributed to electron scattering at Al vacancies with a concentration of 6.4% per site, as quantified by Rutherford back scattering and X-ray reflectivity. Transport measurements at 77 K confirm that $\rho_o\lambda = (12 \pm 1) \times 10^{-16}$ Ωm² is temperature-independent. This value is 79 % larger than for Cu, indicating a more pronounced resistivity size effect in $CuAl_2$. Thus, $CuAl_2$ is only promising as Cu-replacement interconnect metal if its low melting point facilitates large grains and its high cohesive energy provides reliability benefits and an associated reduction in liner thickness.**

***Index Terms*—Cu replacement, interconnects, mean free path, resistivity scaling, $CuAl_2$, surface scattering.**

I. Introduction

Downscaling of conventional Cu interconnects in integrated circuits represents a major challenge because the resistivity increases steeply as the half-pitch is reduced to below the electron mean free path, causing an increasing resistance-capacitance delay [1]-[4]. The resistivity increase in narrow metal lines is primarily due to electron scattering at surfaces and grain boundaries, and is typically described by the Fuchs and Sondheimer (FS) [5], [6] and the Mayadas and Shatzkes (MS) [7] models, respectively. These models suggest that a conductor with a reasonably small bulk resistivity ρ_o and a small bulk electron mean free path λ may exhibit a higher conductivity than Cu in the limit of narrow wires, if the product $\rho_o \times \lambda$ of this conductor is smaller than for Cu [8], [9]. The search for possible Cu replacement materials has initially focused on elemental metals like Co [10], Ru [11], [12], and W [13], with Ru exhibiting a particularly promising combination of low resistivity and excellent reliability for sub-5 nm interconnects [14]-[16]. More recent research includes low-resistivity binary and ternary compounds which exhibit a high cohesive energy and therefore promise a high reliability as potential interconnect conductor [17]. This includes transition metal aluminides and especially $CuAl_2$, which has a good expected resistivity scaling and favorable wetting properties [18], [19]. Additionally, reported capacitance-voltage (C-V) tests and time-dependent-dielectric-breakdown (TDDB) evaluations of $CuAl_2$ on thermal-SiO_2/p-Si substrates indicate good reliability in comparison to conventional Cu/TaN structures [20], suggesting that $CuAl_2$ may facilitate reduced liner/barrier widths or even barrierless $CuAl_2$ interconnects, with a corresponding conductance benefit. On the other hand, open questions remain regarding the effects of the $CuAl_2$ crystallinity and grain structure, surface oxidation, and deviations from stoichiometry on the $CuAl_2$ line resistivity and reliability. Most importantly, the intrinsic resistivity size effect in $CuAl_2$ is not established yet, which motivates our study on the electron transport in thin epitaxial $CuAl_2$ layers.

In this paper, we report on the resistivity scaling in $CuAl_2$ ($Fm\bar{3}m$) as measured using epitaxial $CuAl_2(001)$/MgO(001) layers. Epitaxial single-crystal layers are used because the absence of grain boundaries eliminates the confounding effects from electron grain boundary scattering and facilitates direct quantification of the electron mean free path which is the primary metric used to quantify the resistivity size effect. We use *in situ* transport measurements to avoid possible effects of surface oxidation on the resistivity and possible Al segregation induced by the oxidation. We determine λ = 15.6 nm by fitting the measured ρ vs layer thickness d with the classical FS model [5], [6]. The corresponding $\rho_o\lambda = (12 \pm 1) \times 10^{-16}$ Ωm² is temperature independent, as confirmed by measurements at 77 K, and is 28% larger than the prediction of 9.34×10^{-16} Ωm² from first-principles calculations [21]. Thus, $CuAl_2$ exhibits a slightly larger resistivity size effect than Cu and is therefore only promising as future interconnect metal if it facilitates elimination or a thickness reduction of the liner.

II. Procedure

$CuAl_2$ thin films were deposited in a three-chamber ultra-high vacuum DC magnetron sputtering system with a base pressure < 10^{-9} Torr [22]. Polished 1×1 cm² MgO(001) substrates were cleaned in sequential ultrasonic baths [23] and degassed in vacuum at 1000 °C for 1 hour. Subsequent depositions were done in 3 mTorr 99.999% pure Ar, using constant powers of 120 and 30 W applied to 5-cm-diameter 99.9995 % Al and 99.999 % Cu targets which were facing the substrate at -45 and +45 tilts, yielding a deposition rate of 0.24

The authors acknowledge funding from SRC under task No. 2966.003, the NY State Empire State Development's Division of Science, Technology and Innovation (NYSTAR) through Focus Center-NY–RPI Contract C180117, and the NSF under grant No. 1712752.

The authors are with the Department of Materials Science and Engineering, Rensselaer Polytechnic Institute, 110 8th St, Troy, NY 12180, USA.
Corresponding author: Daniel Gall; email: galld@rpi.edu

nm/s. The substates were continuously rotated to maximize compositional uniformity and were kept at 300 °C which was the optimal temperature to facilitate epitaxial layer growth, good crystalline quality, low surface roughness, and negligible secondary phase formation. The deposition time was adjusted to obtain a series of $CuAl_2$ films with thickness d = 10.2 - 141 nm, as measured by X-ray reflectivity (XRR) for d < 100 nm. The thickness of thicker samples was determined from the deposition rate measured from thinner samples because no XRR oscillations can be resolved for d > 100 nm. After cooling down to room temperature, the samples were transferred in vacuum to the analysis chamber for *in situ* resistivity measurements using a linear four-point probe with a 1 mm inter-probe spacing. For each sample, five measurements with different currents ranging from 1-100 mA were performed and the resistivity was determined from the fitted voltage-vs-current slope.

X-ray diffraction (XRD) and XRR measurements were done in a Panalytical X'pert PRO MPD system with a Cu Kα source using a 45 kV accelerating voltage and a 40 mA current. Symmetric θ-2θ scans were obtained using a parallel beam geometry with an X-ray mirror and a PIXcel solid-state line detector with a 0.165 mm active length acting as a point detector. ω rocking curves were obtained with the same optics. Azimuthal φ-scans were obtained at constant χ and 2θ angles using a point source in combination with an X-ray lens yielding a quasi-parallel beam with an equatorial and axial divergence of 0.3°. Rutherford Backscattering Spectrometry (RBS) was conducted using a linear Dynamitron ion accelerator providing a 2 MeV $^4He^+$ ion beam. Backscattered particles were collected with a Si surface barrier detector at a scattering angle of 166°. The Cu and Al atomic areal densities were obtained from RBS spectra using the SIMNRA simulation software [24].

III. Results and Discussion

Figure 1(a) shows XRR results from a nominally 72-nm-thick $CuAl_2$(001)/MgO(001) layer. The measured intensity is plotted as solid line in a logarithmic scale as a function of the scattering angle 2θ. Data fitting yields the dotted line which is offset by a factor of 0.2 for clarity purposes. It describes the measured data well and corresponds to a 69.8-nm-thick $CuAl_2$ layer covered by a 3.3-nm-thick surface oxide. This oxide has a comparable thickness to what has been reported for room-temperature native surface oxides on Cu or Al, with typical thicknesses of 2.5 – 3.5 nm [25], [26]. We note that the as-deposited $CuAl_2$ layer thickness is larger than the measured thickness, because surface oxide formation consumes a fraction of the Cu and Al atoms. To estimate this effect, we assume that the stoichiometric Cu:Al = 1:2 ratio is retained during surface oxidation and that the resulting CuO-Al_2O_3 surface oxide has an estimated density of 5.15 g/cm^3 which is the average of the CuO and Al_2O_3 densities. Correspondingly, the measured oxide thickness d_{ox} = 3.3 nm is converted into a consumed $CuAl_2$ thickness of 2.5 ± 0.7 nm, yielding an as-deposited d_a = 72.3 ± 1.1 nm. We note that the uncertainty in the as-deposited thickness is larger than for the measured thickness after air exposure. This is because the determination of the consumed $CuAl_2$ thickness adds uncertainty as the surface oxide composition is unknown and may range from Cu oxide to Al oxide. The XRR curve fitting also yields values for the root-mean-square (RMS) roughness of 0.7 ± 0.2 nm for the top surface, 0.4 ± 0.1 nm for the oxide-$CuAl_2$ interface, and 1.5 ± 0.3 nm for the interface between the $CuAl_2$ layer and the MgO(001) substrate, suggesting negligible chemical reaction at the layer-substrate interface. Similar XRR measurements and analyses are performed for all samples. The resulting thickness values for as-deposited and air exposed layers are listed in Table I and are used below to determine the *in situ* and *ex situ* resistivity, respectively.

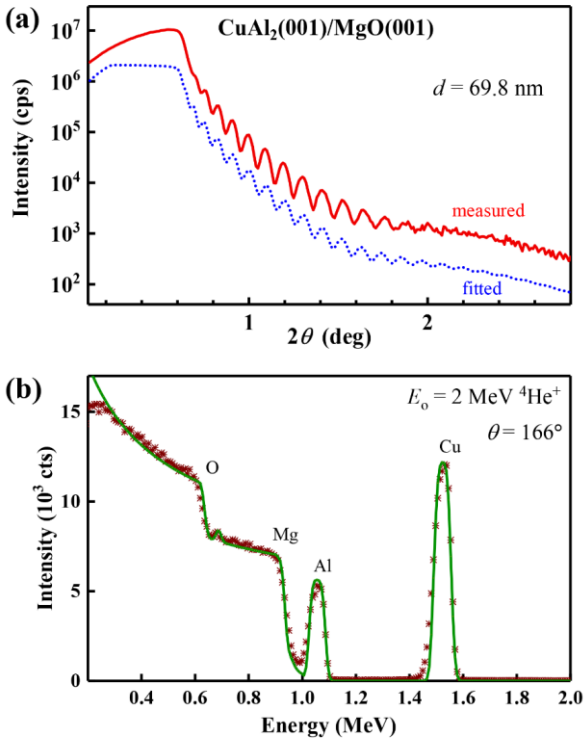

Figure 1. Representative (a) XRR scan including result from curve fitting and (b) measured Rutherford backscattering intensity (brown stars) and simulated spectrum (green curve) for a 69.8-nm-thick epitaxial $CuAl_2$(001)/MgO(001) layer.

Figure 1(b) shows a typical RBS spectrum from the same sample. The measured backscattered intensity vs particle energy is plotted as brown stars and the green curve is the result from curve fitting. The areas under the measured peaks yield total area-densities of Cu and Al atoms of (1.55 ± 0.05) and (2.77 ± 0.09) × 10^{17} atoms/cm^2, indicating a composition with 36 % Cu and 64 % Al which is close to the stoichiometric 33% Cu and 67% Al. We note that a defect-free fully dense stoichiometric $CuAl_2$ layer with a thickness of 72.3 nm (as determined by XRR) has expected Cu and Al atomic densities of (1.50 ± 0.02) and (3.01 ± 0.04) × 10^{17} atoms/cm^2, respectively. The measured values are 3.2% above and 8.0% below these expected densities, indicating a 3.2% excess of Cu atoms which may form anti-site defects and occupy 1.6% of the Al-sites. Conversely, the 8.0% deficiency in Al atoms yields a 6.4% vacancy density on Al-sites. The spectrum in Fig. 1(b) also has a small peak at 0.69 MeV which is attributed to surface oxygen. Curve fitting indicates (2.4 ± 0.9) × 10^{16} oxygen atoms/cm^2 which corresponds to a stoichiometric oxide thickness of 3.4 ± 1.0 nm, consistent with the 3.3-nm-thick surface oxide measured by XRR. We note that the high vapor

pressure of Al makes deposition of stoichiometric $CuAl_2$ challenging as a fraction of deposited Al atoms evaporate at the 300 °C deposition temperature. In addition, previous studies [18], [27] suggest that Al diffusion in aluminide intermetallic compounds facilitates Al surface segregation, preferential Al surface oxidation and a resulting change in composition during air exposure.

Figure 2 shows representative XRD results from the same 69.8-nm-thick $CuAl_2(001)$ layer used for Fig. 1. The θ-2θ pattern in Fig. 1(a) shows a strong doublet feature at 42.92° and 43.04° from MgO 002 substrate reflections of the Cu $K_{\alpha1}$ and $K_{\alpha2}$ x-rays and layer peaks at θ = 15.59° and 31.57° that are ascribed to the $CuAl_2$ 001 and 002 reflections. These peaks confirm the formation of the ordered $CuAl_2$ compound and indicate a measured out-of-plane lattice constant of 5.67 Å. This value is 1.8 % smaller than the reported 5.77 Å [28], which may be attributed to deviations from stoichiometry (in particular Al vacancies) and/or an in-plane biaxial tensile stress caused by the lattice mismatch with the MgO substrate or differential thermal contraction after deposition as the expansion coefficients are 1.3×10^{-5} K^{-1} for MgO [29] and 2.0×10^{-5} K^{-1} for $CuAl_2$ [30]. We note that the $CuAl_2$ 001 reflection is forbidden for the perfect stoichiometric $CuAl_2$ lattice, indicating a considerable point-defect concentration in our samples which breaks the translational symmetry, consistent with the RBS compositional analysis which indicates Al vacancies. The $CuAl_2$ 004 reflection is expected at 2θ = 64.83° but is too weak to be detected for all layers and is therefore not included in Figure 2(a). No other peaks can be detected over the entire measured 2θ = 10-80° range, indicating a $CuAl_2$ 001 orientation along the growth direction without detectable misoriented grains or secondary phases.

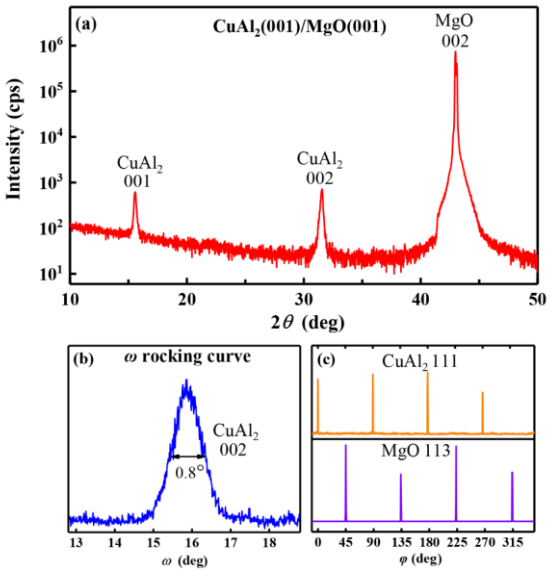

Figure 2. Representative (a) θ-2θ diffractogram, (b) ω rocking curve of the $CuAl_2$ 002 reflection, and (c) φ-scans of the $CuAl_2$ 111 and MgO 113 reflections, from a 69.8-nm-thick epitaxial $CuAl_2(001)$/MgO(001) layer.

The 001-orientation is confirmed by the ω rocking curve shown in Fig. 2(b), obtained using a fixed 2θ = 31.57° to detect the $CuAl_2$ 002 reflection. It exhibits a 0.8° full-width at half maximum (FWHM), indicating good crystalline alignment and an in-plane X-ray coherence length of 21 nm. Fig. 2(c) shows XRD azimuthal φ-scans of MgO 113 and $CuAl_2$ 111 reflections. The bottom pattern is obtained by tilting the sample by χ = 25.23° and fixing 2θ = 74.74°. This yields four peaks at φ = 45, 135, 225, 315°, as expected for a single-crystal MgO(001) substrate. The top pattern is acquired with χ = 54.74° and 2θ = 26.76° to detect $CuAl_2$ 111 reflections. This results in four-fold symmetric peaks at φ = 0, 90, 180, 270°, indicating a single in-plane orientation of the $CuAl_2(001)$ layer. The peak width in φ is < 1.5° for all four peaks, indicating a strong in-plane crystalline alignment of the $CuAl_2$ layer with a maximum in-plane angular spread of 1.5°. These results demonstrate, together with Figs. 2(a) and (b), a 45°-rotated epitaxial layer-substrate relationship with $CuAl_2(001)$ || MgO(001) and $CuAl_2(100)$ || MgO(110). XRD analyses from other $CuAl_2$/MgO(001) layers with different thickness (not shown) exhibit similar results, confirming that all $CuAl_2(001)$ layers presented in this study are epitaxial single-crystal thin films with no detectable secondary phases or misoriented grains. Correspondingly, the following discussion on electron transport neglects any possible contribution from grain boundary scattering.

Figure 3 shows the resistivity ρ vs thickness d of epitaxial $CuAl_2(001)$ layers measured *in situ* at room temperature (295 K) and in liquid N_2 at 77 K, plotted as red squares and blue triangles, respectively. The $CuAl_2(001)$ layer with the largest d = 141 nm has a resistivity of 7.9 ± 0.2 μΩ cm. This is 21 % larger than the reported bulk resistivity of 6.5 μΩ cm [31]. We attribute this deviation to Al vacancies as discussed above. The measured room-temperature resistivity increases with decreasing layer thickness and reaches ρ = 12.6 ± 0.4 μΩ cm for d =10.2 nm, as also presented in Table I. This increase is attributed to electron-surface scattering as quantified in more detail below. We note that our attempt to grow a 5-nm-thick $CuAl_2$/MgO(001) layer led to an infinite resistance due to a discontinuous microstructure, indicating that a nominal thickness of 5 nm is insufficient for nuclei coalescence at the 300 °C growth temperature.

Table I also includes the resistivity measured *ex situ*, that is, after exposure to air. The *ex situ* values are 6 - 13 % larger than the *in situ* resistivity for all layers. This increase is most pronounced for the thinnest layers, suggesting that the effect from air exposure is primarily a surface effect. Similar resistance increases during air exposure have been previously reported for multiple metals including Cu [32], [33], Co [10], [34], Ni [35], Ag [36], and Nb [37] and have been attributed to a surface potential perturbation which causes more diffuse electron scattering. In contrast, the resistivity of more electronegative metals including Ru [11], Rh [38], [39], Ir [40], and W [41] is less affected by air exposure [42]. Similarly, we attribute the resistivity increase during air exposure of our $CuAl_2$ layers to an increase in diffuse electron surface scattering and note that air exposure also causes a 3-10% reduction in the conductive cross-sectional area of the layers since a fraction of the metal is consumed by the growing surface oxide, as quantified by XRR measurements. The latter causes an increase in the measured *ex situ* sheet resistance but does not contribute to the listed resistivity increase because the *in situ* and *ex situ* resistivities in Table I are determined using the as-deposited and measured layer thicknesses, respectively. Nevertheless, in the following, we use primarily the *in situ* resistivity values to quantify the intrinsic $CuAl_2$ resistivity size effect since the

resistivity of air exposed samples may also be affected by surface oxidation induced segregation [43] and roughness [44].

The $CuAl_2$(001) resistivity at 77 K is plotted in Fig. 3 as blue triangles. It exhibits a similar increase with decreasing thickness, from ρ = 2.2 ± 0.1 μΩ cm for d = 141 nm to 7.1 ± 0.4 μΩ cm for d = 9.2 nm. The low-temperature values are 5.5-6.0 μΩ cm below those at room temperature. This difference is (within experimental uncertainty) independent of d and is attributed to an approximately additive resistivity contribution from electron-phonon scattering. We note that the smaller bulk resistivity at 77 K results in a larger relative resistivity size effect. More specifically, the room-temperature resistivity increases by 69% as d is reduced from 141 to 10.2 nm, while the corresponding increase is 223% at 77 K.

The solid lines through the data points are the result from curve fitting using the integral form of the FS model [5], [6]. This is done by setting the specularity parameters p_1 and p_2 for both the top surface and bottom MgO-$CuAl_2$ interfaces to zero. This approach has previously been applied to quantify the resistivity size effect in epitaxial Ir [40], Rh [38], Co [10], Ru [11], and Ti_4SiC_3 [45] layers and yields a λ value which can be understood as an upper bound to possible λ-values or alternatively as the bulk electron mean free path for the case of completely diffuse surface scattering. Data fitting of the room temperature resistivity yields a bulk resistivity ρ_o = 7.7 ± 0.2 μΩ cm and λ = 15.6 ± 1.2 nm. Correspondingly, analysis of the low temperature data yields ρ_o = 2.1 ± 0.1 μΩ cm and λ = 59 ± 4 nm at 77 K. The corresponding product $\rho_o\lambda$ = (11.9 ± 1.0) and (12.9 ± 1.0) × 10^{-16} Ωm^2 at 295 and 77 K, respectively. These two values are identical within experimental uncertainty, suggesting that $\rho_o\lambda$ is temperature independent, as expected from classical transport models [8]. We use in the following and in the abstract a rounded value $\rho_o\lambda$ = 12 × 10^{-16} Ωm^2, where the significant figures indicate the ± 1 uncertainty. This $\rho_o\lambda$ value is 28 % larger than the previously predicted $\rho_o\lambda$ = 9.34 × 10^{-16} Ωm^2 from first-principles calculations [21]. This deviation is relatively small and within the typical range (25-45%) of many metals which show considerably larger effective electron mean free paths from measured ρ vs d data than from first-principles calculations [8]. The larger experimental λ values in comparison to first-principles predictions have previously been attributed to experimental roughness [41], [44], misfit dislocations at the MgO-layer interface that increase the measured effective mean free path, anisotropy in the electron-phonon scattering cross sections [8], or the breakdown of the classical FS model at small dimensions [46].

Our measured $\rho_o\lambda$ = 12 × 10^{-16} Ωm^2 for $CuAl_2$ is 79 % and 135 % larger than for Cu [2] and Ru [11], respectively, and comparable to $\rho_o\lambda$ values for Co [10] and W [13]. Thus, $CuAl_2$ does not provide an intrinsic conductance advantage in comparison to other metals for narrow interconnects. Nevertheless, $CuAl_2$ exhibits some key advantages: (1) $CuAl_2$ has a considerably lower melting point T_m = 592 °C [47] than competing metals like Cu, W, Ru and Co with T_m > 1000 °C. The low melting point facilitates $CuAl_2$ grain growth during annealing at back-end-of-line compatible temperatures. This, in turn, results in an expected $CuAl_2$ conductance benefit as competing metals exhibit substantial resistance contributions from electron scattering at grain boundaries [2], [8], [48], [49]. (2) $CuAl_2$ has a higher cohesive energy than Cu [19] and therefore a higher expected resistance against electromigration and diffusion into the dielectric, and possibly also against oxidation during typical 400 °C back-end-of-line annealing steps. Thus, $CuAl_2$ shows promise as a potential liner-free interconnect metal with the associated conductance benefits. This is supported by previously reported TDDB measurements which found a longer lifetime for $CuAl_2$ in direct contact with SiO_2 than for Cu with a TaN barrier layer [20].

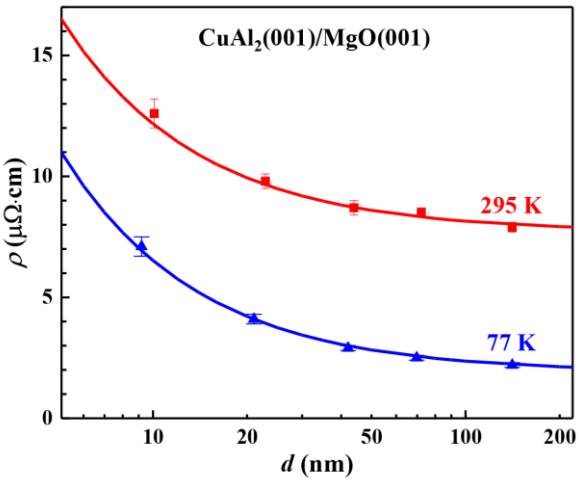

Figure 3. Resistivity ρ vs thickness d of epitaxial $CuAl_2$(001) films measured *in situ* (in vacuum) at 295 K and in liquid N_2 at 77 K.

d_m (nm)	d_{ox} (nm)	d_a (nm)	ρ (μΩ cm)		
			295 K		77 K
			In situ	*Ex situ*	
141 ± 4	—		7.9 ± 0.2	8.4 ± 0.2	2.2 ± 0.1
69.8 ± 0.9	3.3	72.3 ± 1.1	8.5 ± 0.2	9.3 ± 0.3	2.5 ± 0.1
42.1 ± 0.5	2.3	43.8 ± 0.6	8.7 ± 0.3	9.7 ± 0.3	2.9 ± 0.1
21.1 ± 0.3	2.5	23.0 ± 0.4	9.8 ± 0.3	10.5 ± 0.4	4.1 ± 0.2
9.2 ± 0.2	1.4	10.2 ± 0.3	12.6 ± 0.4	14.2 ± 0.7	7.1 ± 0.4

Table I. Measured layer thickness d_m, surface oxide thickness d_{ox}, as-deposited thickness d_a prior to air exposure, and resistivity measured *in situ* in vacuum and *ex situ* after air exposure at 295 K, and immersed in liquid N_2 at 77 K, from epitaxial $CuAl_2$(001)/MgO(001) layers.

IV. Conclusions

$CuAl_2$ layers that are sputter deposited onto MgO(001) substrates at 300 °C are epitaxial layers with $CuAl_2$(001) || MgO(001) and $CuAl_2$(100) || MgO(110), as determined by XRD. Compositional analyses by RBS in combination with XRR show that air exposure causes a 1.4-3.3 nm thick surface oxide. They also reveal an Al vacancy concentration of 6.4% per Al site. *In situ* transport measurements indicate a resistivity increase with decreasing layer thickness that is best described by a bulk electron mean free path λ = 15.6 nm with a bulk resistivity ρ_o = 7.7 μΩ cm. The corresponding values for electron transport at 77 K are λ = 59 nm and ρ_o = 2.1 μΩ cm, yielding an overall product $\rho_o\lambda$ = 12 × 10^{-16} Ωm^2 which is independent of temperature. The overall results suggest that $CuAl_2$ has a more pronounced resistivity size effect than Cu and a comparable resistivity scaling as Co and W. Thus, $CuAl_2$ is only promising as interconnect material if its high cohesive energy facilitates reduction or elimination of a liner/barrier layer.

References

[1] J. Chawla, D. Gall, "Specular electron scattering at single-crystal Cu (001) surfaces," *Appl. Phys. Lett.,* vol. *94*, no. 25, p. 252101, Jun. 2009, doi: 10.1063/1.3157271.

[2] J. Chawla, F. Gstrein, K. O'Brien, J. Clarke, D. Gall, "Electron scattering at surfaces and grain boundaries in Cu thin films and wires," *Phys. Rev. B,* vol. *84*, no. 23, p. 235423, Dec. 2011, doi: 10.1103/PhysRevB.84.235423.

[3] P. Kapur, J. P. McVittie, K. C. Saraswat, "Technology and reliability constrained future copper interconnects. I. Resistance modeling," *IEEE Trans. Electron Devices,* vol. *49*, no. 4, pp. 590-597, Apr. 2002, doi: 10.1109/16.992867.

[4] D. Gall, J. J. Cha, Z. Chen, H.-J. Han, C. Hinkle, J. A. Robinson, R. Sundararaman, R. Torsi, "Materials for interconnects," *MRS Bull.,* vol. *46*, no. 10, pp. 959-966, Oct. 2021, doi: 10.1557/s43577-021-00192-3.

[5] K. Fuchs "The conductivity of thin metallic films according to the electron theory of metals," in *Math. Proc. Cambridge Philos. Soc.*, Jan. 1938; pp. 100-108 doi: 10.1017/S0305004100019952.

[6] E. H. Sondheimer, "The mean free path of electrons in metals," *Adv. Phys.,* vol. *1*, no. 1, pp. 1-42, Jan. 1952, doi: 10.1080/00018735200101151.

[7] A. Mayadas, M. Shatzkes, "Electrical-resistivity model for polycrystalline films: the case of arbitrary reflection at external surfaces," *Phys. Rev. B,* vol. *1*, no. 4, p. 1382, Feb. 1970, doi: 10.1103/PhysRevB.1.1382.

[8] D. Gall, "The search for the most conductive metal for narrow interconnect lines," *J. Appl. Phys.,* vol. *127*, no. 5, p. 050901, Feb. 2020, doi: 10.1063/1.5133671.

[9] D. Gall, "Electron mean free path in elemental metals," *J. Appl. Phys.,* vol. *119*, no. 8, p. 085101, Feb. 2016, doi: 10.1063/1.4942216.

[10] E. Milosevic, S. Kerdsongpanya, M. E. McGahay, A. Zangiabadi, K. Barmak, D. Gall, "Resistivity scaling and electron surface scattering in epitaxial Co (0001) layers," *J. Appl. Phys.,* vol. *125*, no. 24, p. 245105, Jun. 2019, doi: 10.1063/1.5086458.

[11] E. Milosevic, S. Kerdsongpanya, A. Zangiabadi, K. Barmak, K. R. Coffey, D. Gall, "Resistivity size effect in epitaxial Ru (0001) layers," *J. Appl. Phys.,* vol. *124*, no. 16, p. 165105, Oct. 2018, doi: 10.1063/1.5046430.

[12] S. S. Ezzat, P. D. Mani, A. Khaniya, W. Kaden, D. Gall, K. Barmak, K. R. Coffey, "Resistivity and surface scattering of (0001) single crystal ruthenium thin films," *J. Vac. Sci. Technol., A,* vol. *37*, no. 3, p. 031516, May 2019, doi: 10.1116/1.5093494.

[13] P. Zheng, D. Gall, "The anisotropic size effect of the electrical resistivity of metal thin films: Tungsten," *J. Appl. Phys.,* vol. *122*, no. 13, p. 135301, Oct. 2017, doi: 10.1063/1.5004118.

[14] L. G. Wen, C. Adelmann, O. V. Pedreira, S. Dutta, M. Popovici, B. Briggs, N. Heylen, K. Vanstreels, C. J. Wilson, S. Van Elshocht "Ruthenium metallization for advanced interconnects," in *2016 IEEE International Interconnect Technology Conference/Advanced Metallization Conference (IITC/AMC)*, May 2016; pp. 34-36 doi: 10.1109/IITC-AMC.2016.7507651.

[15] X. Zhang, H. Huang, R. Patlolla, W. Wang, F. W. Mont, J. Li, C.-K. Hu, E. G. Liniger, P. S. McLaughlin, C. Labelle "Ruthenium interconnect resistivity and reliability at 48 nm pitch," in *2016 IEEE International Interconnect Technology Conference/Advanced Metallization Conference (IITC/AMC)*, May 2016; pp. 31-33 doi: 10.1109/IITC-AMC.2016.7507650.

[16] E. Milosevic, S. Kerdsongpanya, D. Gall "The resistivity size effect in epitaxial Ru (0001) and Co (0001) layers," in *2018 IEEE Nanotechnology Symposium (ANTS)*, Nov. 2018; pp. 1-5 doi: 10.1109/NANOTECH.2018.8653560.

[17] K. Sankaran, K. Moors, Z. Tőkei, C. Adelmann, G. Pourtois, "Ab initio screening of metallic MAX ceramics for advanced interconnect applications," *Phys. Rev. Mater.,* vol. *5*, no. 5, p. 056002, May 2021, doi: 10.1103/PhysRevMaterials.5.056002.

[18] J.-P. Soulié, Z. Tőkei, J. Swerts, C. Adelmann "Aluminide intermetallics for advanced interconnect metallization: thin film studies," in *2021 IEEE International Interconnect Technology Conference (IITC)*, Jul. 2021; pp. 1-3 doi: 10.1109/IITC51362.2021.9537441.

[19] L. Chen, D. Ando, Y. Sutou, J. Koike, "CuAl2 thin films as a low-resistivity interconnect material for advanced semiconductor devices," *J. Vac. Sci. Technol., B,* vol. *37*, no. 3, p. 031215, May 2019, doi: 10.1116/1.5094404.

[20] T. Kuge, M. Yahagi, J. Koike "Effects of composition deviation of CuAl 2 on BTS and TDDB reliability," in *2021 IEEE International Interconnect Technology Conference (IITC)*, Jul. 2021; pp. 1-3 doi: 10.1109/IITC51362.2021.9537528.

[21] L. Chen, S. Kumar, M. Yahagi, D. Ando, Y. Sutou, D. Gall, R. Sundararaman, J. Koike, "Interdiffusion reliability and resistivity scaling of intermetallic compounds as advanced interconnect materials," *J. Appl. Phys.,* vol. *129*, no. 3, p. 035301, Jan. 2021, doi: 10.1063/5.0026837.

[22] B. Wang, D. Gall, "Fully strained epitaxial Ti1− xMgxN (001) layers," *Thin Solid Films,* vol. *688*, no. p. 137165, Oct. 2019, doi: 10.1016/j.tsf.2019.02.028.

[23] P. Fang, B. Wang, D. Gall, "Epitaxial MoCx: Competition between cubic δ-MoCy (111) and hexagonal β-Mo2C (0001)," *Surf. Coat. Technol.,* vol. no. p. 127333, Aug. 2021, doi: 10.1016/j.surfcoat.2021.127333.

[24] M. Mayer, "Improved physics in SIMNRA 7," *Nuclear Instruments and Methods in Physics Research Section B: Beam Interactions with Materials and Atoms,* vol. *332*, no. 1, pp. 176-180, Aug. 2014, doi: j.nimb.2014.02.056.

[25] W. B. Frank, W. E. Haupin, H. Vogt, M. Bruno, J. Thonstad, R. K. Dawless, H. Kvande, O. A. Taiwo, "Aluminum," *Ullmann's Encyclopedia of Industrial Chemistry,* vol. no. Jun. 2000, doi: 10.1002/14356007.a01_459.

[26] C. K. Chung, Y. Chen, C. Li, C. Kao, "The critical oxide thickness for Pb-free reflow soldering on Cu substrate," *Thin Solid Films,* vol. *520*, no. 16, pp. 5346-5352, Jun. 2012, doi: 10.1016/j.tsf.2012.03.034.

[27] N. Cai, H. Qin, X. Tong, G. Zhou, "Growth of ultrathin amorphous alumina films during the oxidation of NiAl (100)," *Surf. Sci.,* vol. *618*, no. pp. 20-26, Dec. 2013, doi: 10.1016/j.susc.2013.09.011.

[28] A. Jain, S. P. Ong, G. Hautier, W. Chen, W. D. Richards, S. Dacek, S. Cholia, D. Gunter, D. Skinner, G. Ceder, "Commentary: The Materials Project: A materials genome approach to accelerating materials innovation," *APL materials,* vol. *1*, no. 1, p. 011002, Jul. 2013, doi: 10.1063/1.4812323.

[29] D. Gall, I. Petrov, N. Hellgren, L. Hultman, J. Sundgren, J. Greene, "Growth of poly-and single-crystal ScN on MgO (001): Role of low-energy N 2+ irradiation in determining texture, microstructure evolution, and mechanical properties," *J. Appl. Phys.,* vol. *84*, no. 11, pp. 6034-6041, Nov. 1998, doi: 10.1063/1.368913.

[30] C. Macchioni, J. Rayne, S. Sen, C. Bauer, "Low temperature resistivity of thin film and bulk samples of CuAl2 and Cu9Al4," *Thin Solid Films,* vol. *81*, no. 1, pp. 71-78, Jul. 1981, doi: 10.1016/0040-6090(81)90506-X.

[31] J. Gniewek, C. Wasik, "Electrical Resistivity and Hall Coefficient of CuAl2," *J. Appl. Phys.,* vol. *42*, no. 5, pp. 2151-2151, 1971, doi: 10.1063/1.1660512.

[32] P. Zheng, R. Deng, D. Gall, "Ni doping on Cu surfaces: Reduced copper resistivity," *Appl. Phys. Lett.,* vol. *105*, no. 13, p. 131603, Sep. 2014, doi: 10.1063/1.4897009.

[33] J. Chawla, F. Zahid, H. Guo, D. Gall, "Effect of O 2 adsorption on electron scattering at Cu (001) surfaces," *Appl. Phys. Lett.,* vol. *97*, no. 13, p. 132106, Sep. 2010, doi: 10.1063/1.3489357.

[34] E. Milosevic, D. Gall, "Electron scattering at Co (0001) surfaces: Effects of Ti and TiN capping layers," *AIP Adv.,* vol. *10*, no. 5, p. 055213, May 2020, doi: 10.1063/1.5145327.

[35] E. Milosevic, P. Zheng, D. Gall, "Electron scattering at epitaxial Ni (001) surfaces," *IEEE Trans. Electron Devices,* vol. *66*, no. 10, pp. 4326-4330, Aug. 2019, doi: 10.1109/TED.2019.2934636.

[36] J. Chawla, D. Gall, "Epitaxial Ag (001) grown on MgO (001) and TiN (001): Twinning, surface morphology, and electron surface scattering," *J. Appl. Phys.,* vol. *111*, no. 4, p. 043708, Feb. 2012, doi: 10.1063/1.3684976.

[37] E. Milosevic, S. Kerdsongpanya, M. E. McGahay, B. Wang, D. Gall, "The resistivity size effect in epitaxial Nb (001) and Nb (011) layers," *IEEE Trans. Electron Devices,* vol. *66*, no. 8, pp. 3473-3478, Aug. 2019, doi: 10.1109/TED.2019.2924312.

[38] A. Jog, T. Zhou, D. Gall, "Resistivity Size Effect in Epitaxial Rh (001) and Rh (111) Layers," *IEEE Trans. Electron Devices,* vol. *68*, no. 1, pp. 257-263, Jan. 2021, doi: 10.1109/TED.2020.3040202.

[39] A. Jog, D. Gall, "Electron Scattering at Surfaces and Grain Boundaries in Rh Layers," *IEEE Trans. Electron Devices,* vol. no. Jun. 2022, doi: 10.1109/TED.2022.3177153.

[40] A. Jog, D. Gall, "Resistivity size effect in epitaxial iridium layers," *J. Appl. Phys.,* vol. *130*, no. 11, p. 115103, Sep. 2021, doi: 10.1063/5.0060845.

[41] P. Zheng, T. Zhou, B. Engler, J. Chawla, R. Hull, D. Gall, "Surface roughness dependence of the electrical resistivity of W (001) layers," *J. Appl. Phys.,* vol. *122*, no. 9, p. 095304, Sep. 2017, doi: 10.1063/1.4994001.

[42] A. Jog, E. Milosevic, P. Zheng, D. Gall, "Effect of electronegativity on electron surface scattering in thin metal layers," *Appl. Phys. Lett.,* vol. *120*, no. 4, p. 041601, Jan. 2022, doi: 10.1063/5.0078877.

[43] J.-P. Soulié, Z. Tőkei, J. Swerts, C. Adelmann "Thickness scaling of NiAl thin films for alternative interconnect metallization," in *2020 IEEE International Interconnect Technology Conference (IITC)*, Oct. 2020; pp. 151-153 doi: 10.1109/IITC47697.2020.9515638.

[44] T. Zhou, P. Zheng, S. C. Pandey, R. Sundararaman, D. Gall, "The electrical resistivity of rough thin films: A model based on electron reflection at discrete step edges," *J. Appl. Phys.,* vol. *123*, no. 15, p. 155107, Apr. 2018, doi: 10.1063/1.5020577.

[45] M. Zhang, S. Kumar, R. Sundararaman, D. Gall, "Resistivity scaling in epitaxial MAX-phase Ti4SiC3(0001) layers," *J. Appl. Phys.,* vol. *130*, no. 3, p. 034302, Jul. 2021, doi: 10.1063/5.0054542.

[46] T. Zhou, D. Gall, "Resistivity scaling due to electron surface scattering in thin metal layers," *Phys. Rev. B,* vol. *97*, no. 16, p. 165406, Apr. 2018, doi: 10.1103/PhysRevB.97.165406.

[47] J. L. Murray, "The aluminium-copper system," *Int. Met. Rev.,* vol. *30*, no. 1, pp. 211-234, Jul. 1985, doi: 10.1179/imtr.1985.30.1.211.

[48] T. Zhou, A. Jog, D. Gall, "First-principles prediction of electron grain boundary scattering in fcc metals," *Appl. Phys. Lett.,* vol. *120*, no. 24, p. 241603, Jun. 2022, doi: 10.1063/5.0098822.

[49] M. César, D. Gall, H. Guo, "Reducing grain-boundary resistivity of copper nanowires by doping," *Phys. Rev. Appl.,* vol. *5*, no. 5, p. 054018, May 2016, doi: 10.1103/PhysRevApplied.5.054018.